JET Template_2022_rev1.pdf

by Natalita Maulani

Ground Penetrating Radar Data Inversion Using Dual-Input Convolutional Autoencoder for Ferroconcrete Inspection

Budiman P.A. Rohman[a,b], Masahiko Nishimoto[c], Ratna Indrawijaya[a], Dayat Kurniawan[a], Purwoko Adhi[a], Iman Firmansyah[a]

[a]*Research Center for Telecommunication*
National Research and Innovation Agency (BRIN)
KST Samaun Samadikun, Jl. Sangkuriang
Bandung, Indonesia
[b]*School of Electrical Engineering*
Telkom University
Jl. Telekomunikasi 1
Bandung, Indonesia
[c]*Faculty of Advanced Science and Technology*
Kumamoto University
2-39-1 Kurokami, Chuo Ward
Kumamoto, Japan
Corresponding author: budi057@brin.go.id

Abstract

Ground penetrating radar (GPR) is a non-destructive tool for observing an object buried underground. Currently, GPR is also considered for reinforced concrete inspection. However, the image produced by GPR can not be easily interpreted. Besides, the large observation of building concrete inspection also motivates the researchers to fastening and easing radar image interpretation. Thus, this research proposes GPR scattering data inversion method to produce an internal structure image. The proposed employs a convolutional autoencoder model using amplitude and phase radar data as input of the algorithm. As evaluation, in this stage, we perform numerical analysis by using finite-difference time-domain-based synthetic data that considers three cases: concrete with rebar, concrete with crack, and concrete with rebar and crack. All of those cases are simulated with randomized dimensions and positions that is possible in the real applications. Compared with the baseline method, our method shows superiority, especially in the semantic segmentation perspective. The parameter size of the proposed model is also much smaller, around one-third of the previous method. Therefore, the method is feasible enough to be implemented in real applications addressing an automatic internal structure reinforced concrete mapping.

Keywords: radar, ground penetrating radar, wave inversion, full wave inversion, deep learning, machine learning, autoencoder, convolutional neural networks

I. INTRODUCTION

Ground Penetrating Radar (GPR) is a sensing technology that utilizes electromagnetic waves to investigate information about subsurface objects. When electromagnetic waves travel to the ground, the buried object partially reflects them. These reflected waves are subsequently processed and analyzed to locate the object and ascertain its characteristics. GPR has found application in various fields, including geophysics, geology, archeology, civil engineering and humanitarian demining [1][2]. Of particular interest to researchers currently is the latest application of GPR: non-destructive inspection of concrete structures, as referenced in [3][4] and [5]. However, it is challenging to interpret the recorded data and images from the GPR. Some advanced and complex processing is required. Thus, to fasten and ease the non-destructive inspection data acquisition and interpretation, simple and lightweight data processing is required.

The Full Waveform Inversion (FWI) is the standard method to identify the buried object from GPR signals. Some of the research that proposes that method is as follows. In 2012, Busch et al. proposed the quantitative conductivity and permittivity estimation using FWI [6]. In 2014, Forte et al. analyzed the velocity from common offset GPR data inversion that had been applied in the synthetic and real data [7]. Spectral inversion method on GPR data has been proposed by Huang et al to determine the parameters of subsurface layers [8]. In 2019, Jazayeri made reinforced concrete mapping using FWI of GPR data [9].

Currently, artificial intelligence algorithms, especially Deep Learning (DL), are popular. This algorithm can make a black box that mimics a transformation of any input and output. The use of DL algorithms on the ultrawideband radar image data to reconstruct the internal structure of material became the concern of many researchers. Many of them use deep learning to detect, classify and recognize the buried object in the structure [10-14]. However, currently, the researchers use this technique as a new approach for the radar response inversion problem. The inversion of radar images using deep learning algorithms, such as Enc-Dec, U-Net, and GAN has been conducted by Alvarez et al. [15]. The convolutional-to-trace network has been proposed to reconstruct the image to reconstruct the tunnel lining structure [16]. Ji et al. proposed a deep neural network for inverting the permittivity of GPR data [17]. The use of a convolutional neural network in the architecture SegNet to make the defect segmentation of the buried object in the lining tunnel based on its permittivity values has been proposed by Yang et al [18]. However, implementing those methods in the real GPR data still has some drawbacks and limitations.

In this proposal, we develop a new machine learning structure to improve the previous method's performance. Inspired by the valuable information carried by the phase of the radar signal [8-9] and the success of the previous research in the buried shape reconstruction using this feature [10], in this study, we use both amplitude and phase images of the GPR B-scan data. In this paper, we propose a DL-based inversion method that employs the amplitude and phase of the reflection signal concurrently, aiming at an accurate and light computation model. By combining information carried by amplitude and phase with an appropriate technique, we hypothesize that the developed model can provide a better inversion performance. Besides, from this study, we also can obtain different perspectives in the exploration of the phase information of radar data for image inversion. As an evaluation, we focus on the application of reinforced concrete inspection employing synthetic data based on the finite-difference time-domain method. We use the method from [18] as the baseline of performance and model complexity evaluation.

The remaining of this paper is organized as follows. The proposed method is explained briefly in section II, followed by the numerical analysis setup in section III. The result of the analysis is explained in section IV. Then, the conclusion of this study is described in section V.

II. Proposed Method

A. Ferroconcrete Inspection

In the concrete inspection using GPR (see Fig.1), the GPR works by emitting an electromagnetic pulse through the emission antenna. Thus, the radar waves propagate in the concrete with a speed that depends on the electrical properties of the media, the receiving antenna receives electric fields generated by the internal objects (such as rebar or void) according to the time. The electrical properties that affect significantly in the GPR recorded signal are permittivity (ε) and conductivity (σ). Electrical conductivity conveys the current density information generated by an external electric field, while permittivity is a complex-valued attribute indicating the medium's susceptibility to polarization by external electric fields. The complex permittivity (ε_c) is defined in relation to ε and σ as:

$$\varepsilon_c = \varepsilon - j\frac{\sigma}{\omega} = \varepsilon' - j\varepsilon'' \quad (1)$$

where the real part, $\varepsilon' = \varepsilon$, corresponds to the dielectric constant, while the imaginary part, $\varepsilon'' = \frac{\sigma}{\omega}$, represents the loss factor, indicative of energy dissipation due to absorption. The dielectric constant or relative permittivity, ε_r. This value is obtained by dividing it by the free space permittivity, ε_0=8.854×10^(-12) F/m expressed by:

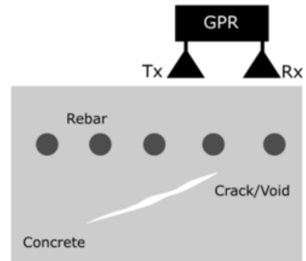

Figure 1. The process of ferroconcrete inspection

$$\varepsilon_r = \frac{\varepsilon}{\varepsilon_0} \quad (1)$$

The alteration in this dielectric constant value is primarily induced by the water content, owing to its high dielectric constant and substantial loss factor [19].

B. Deep Learning Method

Deep Learning (DL) constitutes a sector within machine learning that constructs a nonlinear parametrized mapping by processing through multiple layers to extract high-level features. At the heart of this algorithm is the artificial neural network, which simulates human neurons [19]. If 'f' denotes a function within DL, then:

$$\boldsymbol{Y_P} = f(\boldsymbol{X}, \boldsymbol{\theta}) \quad (1)$$

where Y_P denotes the predicted value, X signifies the input data, and θ symbolizes the parameters of DL, usually encompassing weight and bias values, among other factors. The parameters of the neural network undergo iterative adjustments during the learning phase to minimize the estimation error between the predicted and target values.

C. Dual-Input Convolutional Autoencoder

The deep auto-encoder (AE) is a variation of the feed-forward neural network, primarily designed to compress input data into more condensed representations and then reconstruct the original input data as faithfully as possible using the learned compact representations. This algorithm operates within the unsupervised learning paradigm, where the goal is to make the target values equal to the inputs. Consisting of two symmetric but separate components, an auto-encoder comprises the encoder and the decoder. During the training process, parameters are learned to minimize discrepancies between the original data and the reconstructed outputs through backpropagation.

Convolutional autoencoders (CAE) share a similar architectural pattern with classic autoencoders (AE), incorporating encoding and decoding layers. However, unlike classic AE, which relies on fully connected layers, CAE employs convolutional and max-pooling layers for encoding and decoding. These layers are specifically designed to transform high-dimensional input vectors into lower-dimensional compact feature vectors, with the decoding layers structured using convolutional layers. Key components of this architecture include convolution

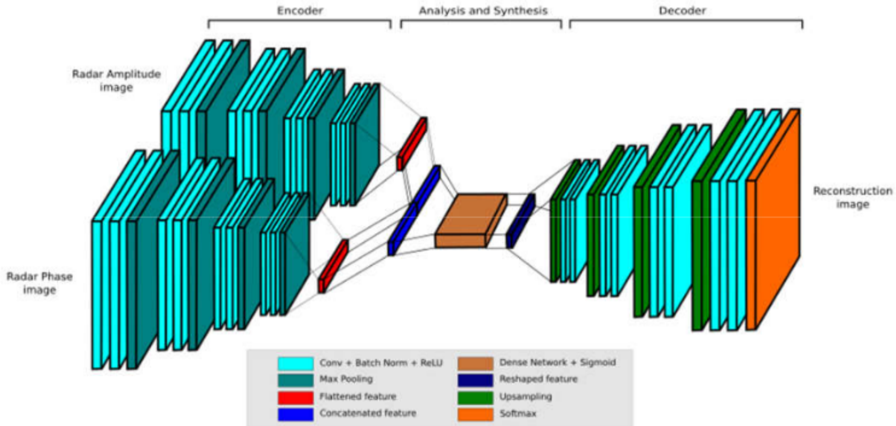

Figure 2. Proposed dual-input convolutional autoencoder

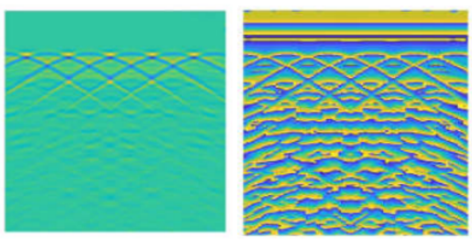

(a) (b)

Figure 3. The amplitude and phase images of GPR data in case 1 used as input of proposed method.

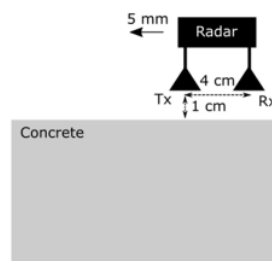

Figure 4. Setup of experiment

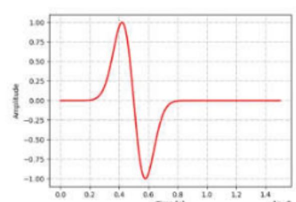

Figure 5. Monocycle pulse exited by GPR

layers, pooling layers, and fully connected layers. Through the application of the backpropagation algorithm, CAE aims to automatically learn spatial hierarchies of features..

In this study, the auto-encoder architecture comprises 4 encoding layers from 2 inputs and 4 decoding layers. The encoding convolutional layer filter number are 8,16,24 and 32, respectively, with filter size of 15 × 15. Each of convolutional layer is followed by Batch Normalization layer, RelU activation unit and Max Pooling layer with size 2×2. After fourth layer encoding, the result from both input are flattened to be processing by dense network with sigmoid activation function.

The next step is decoding process that consists of four layers. The first layer consist of upsampling layer 2×2, convolutional layer with number 32 and filter size of 15×15, a Batch Normalization, and RelU activation function. This layer is followed by the other three layers with the same structure, but their filter number of the convolutional layer are 24, 16, and 8, respectively.

The final layer consists of one convolutional layer with filter size 1x1, Batch normalization, and Softmax activation function.

III. Numerical Analysis Setup

A. Dataset

As a dataset of the model, we use synthetic data generated by gprMax, a finite-difference time-domain-based electromagnetic software [20]. The antenna is the Hertzian dipole antenna placed above concrete around 1 cm that moves forward with a step of 5 mm to produce B-scan. Between the transmitter and receiver antenna, there is a range of 4 cm. The radar uses a monocycle pulse with the center of frequency 2 GHz. The equation of the waveform is defined as

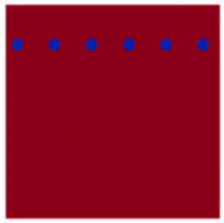

Concrete with rebars

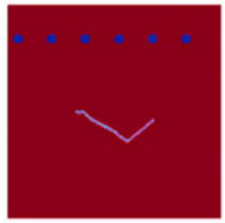

Concrete with rebars and crack

Component	ε_r	σ	Dimension (cm)
Concrete	6-8	0.0001	width =50, height=49
Rebar (PEC)	1	∞	radius=0.5-1.5, space= 4xR
Crack/Void	1	0	length=5-30, width=0.5-2.0

Fig. 6. Simulated model for generating synthetic data.

$$W(t) = -2\sqrt{\frac{e}{2\psi}}\psi(t-\omega)e^{-\psi(t-\omega)^2} \quad (1)$$

where $\psi = 2\pi^2 f^2$, $\omega = \frac{1}{f}$ and f is the radar frequency. The shape of the waveform can be seen in Fig.3

In this study, we consider three conditions of reinforced concrete: concrete with rebars; concrete with rebars and crack; and concrete with crack. The parameters of the object, such as relative permittivity (ε_r) and conductivity (σ) can be seen in Fig. 1. The condition of each component is with various depths, various radii, and various spaces (rebars). Each case has 3000 B-scan data: 2000 for training, 500 data validation, and 500 data for testing in each case. Thus, the total of data we used is 9000 data. The sample of data is shown in Fig.1.

To assess the effectiveness of the proposed model, we employ four standard metrics: accuracy, precision, recall, and F1-score. Accuracy reflects the ratio of correct predictions, computed by dividing the total number of correct predictions by the sum of true positive and false negative occurrences. Precision indicates the model's accuracy in predicting positive classes, calculated by dividing the sum of true positive and false positive occurrences by the total number of positive predictions. Recall measures the ratio of correctly predicted positive classes, determined by dividing the sum of true positive and false negative occurrences by the total number of true positive instances. The F1-score represents the weighted average of recall and precision, with a score of 1 indicating optimal performance and 0 indicating the poorest. These metrics can be expressed as:

$$Accuracy = \frac{TP+TN}{TP+FN+TN+FP} \quad (2)$$

$$Precision = \frac{TP}{TP+FP} \quad (3)$$

$$Recall = \frac{TP}{TP+FN} \quad (4)$$

$$F1-score = \frac{2 \times Precision \times Recall}{Precision + Recall} \quad (5)$$

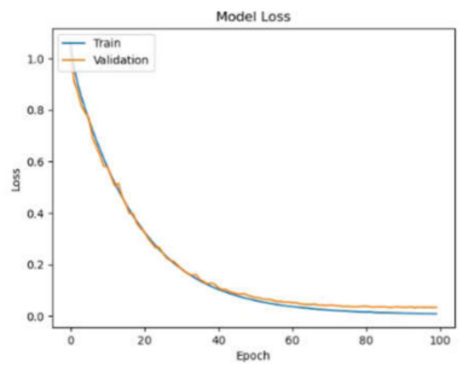

Figure 7. Comparison of model parameter sizes

where TP stands for true positives, TN for true negatives, FP for false positives, and FN for false negatives..

B. Implementation

The proposed model underwent training and testing on a 64-bit Windows 10 Pro workstation equipped with an Intel Core i7-8700K CPU operating at 3.70 GHz with 12 cores. The computer memory is 32 GB of RAM, and the graphic card is an NVIDIA RTX 3060 GPU. The deep learning model was constructed using TensorFlow and Keras frameworks. During the training phase, a mini-batch size of 8 was utilized, alongside a learning rate set at 1^{-2}. The maximum epoch is 100. To prevent overfitting, an early-check mechanism based on validation loss value was integrated into the training process, terminating training when performance ceased to improve, with a delay of 10 epochs.

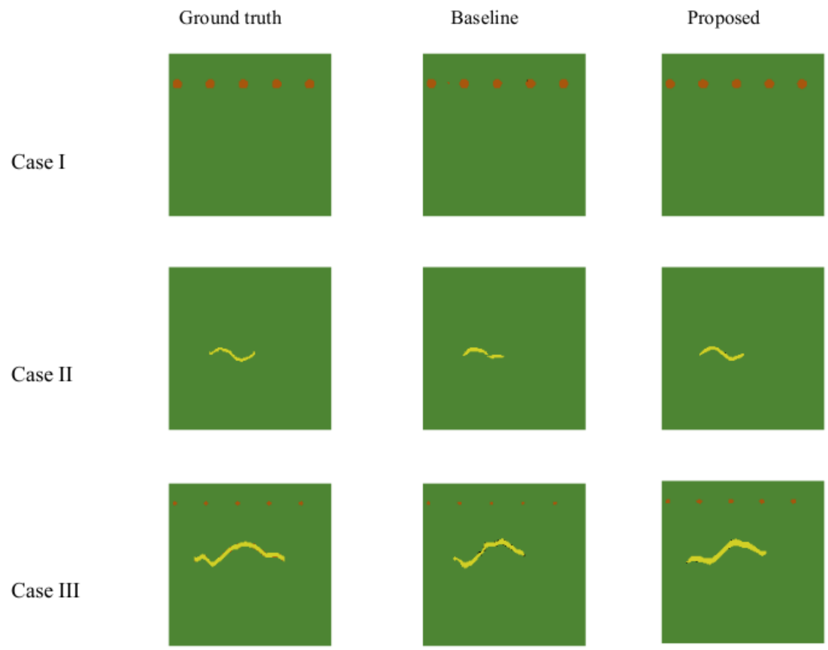

Figure 8. Comparison of inversion result visualization of three observed cases in ground truth with proposed and baseline method results. The color green, orange and yellow indicates concrete, rebar, and crack or void, respectively.

IV. Results

The proposed method performance is evaluated from three perspectives: model training process, inversion result visualization and metrics evaluation. Comparison with the existing method is also taken to see the advancement of the proposed method.

A. Model Training

The loss curve change during data training is shown by Figure 1. From this figure it can be seen clearly that the loss converges around epoch 100 in both tranining and validation data. This figure also confirm that there is No. underfitting or overfitting on the training process.

B. Data Inversion Visualization

Table 1 shows the comparison of inversion results using the baseline and proposed methods. In case I, there is almost no significant difference in the results between baseline and proposed methods. Thus, in this case we can conclude that both methods have the relatively equal performance. However, in the case II and III, it can be seen clearly that the proposed method has better performance especially in the shape and area of the crack. Besides, from those two observations, we also can conclude that the rebars are easy to be detected and inverted. This is caused by the strong reflection from the rebar. Meanwhile, the crack cannot be detected well since the crack reflection is weak, and relatively small. In case III, this signal is also masked by the rebar reflection signals so that the reconstruction result is not as accurate as two previous cases.

Table 2. Comparison of Metrics

Metrics	Case	Accuracy	
		Baseline	Proposed
Accuracy	I	0.9877	**0.9984**
	II	0.9898	**0.9926**
	III	0.9772	**0.9868**
F1	I	0.9877	**0.9984**
	II	0.9899	**0.9984**
	III	0.9772	**0.9868**
Recall	I	0.9877	**0.9984**
	II	0.9898	**0.9927**
	III	0.9772	**0.9866**
Precision	I	0.9877	**0.9984**
	II	0.9899	**0.9927**
	III	0.9772	**0.9870**

Table 3. Comparison of model parameter sizes

Characteristics	Baseline	Proposed
Parameters	61 million	22 million

B. Metrics Evaluation

The superiority of the proposed method in the inversion results is confirmed further by Table 2. This table shows the performance metrics of both methods in the semantic segmentation perspective. From this table, in all cases and metrics, the proposed method has a higher score. Although the difference is relatively small, this still should be considered since the metrics calculate each pixel's values, and the majority of the pixel of the image is concrete. Thus, this result can confirm confidently that the method has better performance than the baseline.

To evaluate further the proposed method, we also compare the model parameter size as in Table 3. As we can see, the proposed method has one third parameter size than the baseline ones. With this smaller parameter size, the proposed can be processed faster. Thus, the method is more feasible to be implemented in real time especially in the case when the complexity and processing time became concern of the GPR operation.

V. CONCLUSION

In this report, we show our study about the use of a dual-input convolutional autoencoder algorithm for mapping the reinforced concrete internal structure. The method employs the amplitude and phase data of the GPR. Compared with the baseline method, the proposed method shows its superiority in almost all observed cases and from qualitative and quantitative perspectives. By its simpler model and superior performance, we show that the proposed method is feasible enough to be applied in real applications, especially in reinforced concrete inspection. Besides, from this study, we also confirm that the phase information on the recorded radar image is useful for the data inversion aiming at the identification of the obscured object.

DECLARATIONS

Conflict of Interest

The authors have declared that no competing interests exist

CRediT Authorship Contribution

Budiman P.A. Rohman: Conceptualization, Methodology, Visualization; Masahiko Nishimoto: Conceptualization, Methodology; Ratna Indrawijaya: Methodology, Investigation; Dayat Kurniawan: Visualization, Investigation, Writing-Reviewing and Editing; Purwoko Adhi: Investigation; Iman Firmansyah: Investigation, Writing-Reviewing and Editing.

ACKNOWLEDGMENT

The part of this study is supported by Research Organization of Electronics and Informatics BRIN under *Rumah Program Sistem Pendukung Keputusan Berbasis Analisis Citra Satelit* program. The authors also would like to thank to Kumamoto University, Japan for the experimentation facilities generating data.

REFERENCE

[1] H. M. Jol, Ground Penetrating Radar Theory and Applications, Elsevier. 2008.

[2] A. Benedetto, and L. Pajewski, eds. Civil engineering applications of ground penetrating radar. Springer, 2015.

[3] M. Nishimoto, BPA Rohman, and Y. Naka. "Estimation of concrete corrosion state using ultra-wideband radar signatures." IGARSS 2019-2019 IEEE International Geoscience and Remote Sensing Symposium. IEEE, 2019.

[4] BPA. Rohman, M. Nishimoto, and K. Ogata. "Material Permittivity Estimation Using Analytic Peak Ratio of Air-Coupled GPR Signatures." IEEE Access 10 (2022): 13219-13228.

[5] B. P. A. Rohman and M. Nishimoto, "Multi-scaled power spectrum based features for landmine detection using Ground Penetrating Radar," 2017 International Conference on Signals and Systems (ICSigSys), Bali, Indonesia, 2017, pp. 83-86.

[6] Busch, Sebastian, et al. "Quantitative conductivity and permittivity estimation using full-waveform inversion of on-ground GPR data." Geophysics 77.6 (2012): H79-H91.

[7] Forte, Emanuele, et al. "Velocity analysis from common offset GPR data inversion: theory and application to synthetic and real data." Geophysical Journal International 197.3 (2014): 1471-1483.

[8] Huang, Zhong-lai, and Jianzhong Zhang. "Determination of parameters of subsurface layers using GPR spectral inversion method." IEEE Transactions on Geoscience and Remote Sensing 52.12 (2014): 7527-7533.

[9] Jazayeri, Sajad, et al. "Reinforced concrete mapping using full-waveform inversion of GPR data." Construction and Building Materials 229 (2019): 117102.

[10] Pham, Minh-Tan, and Sébastien Lefèvre. "Buried object detection from B-scan ground penetrating radar data using Faster-RCNN." IGARSS 2018-2018 IEEE International Geoscience and Remote Sensing Symposium. IEEE, 2018.

[11] Dinh, Kien, Nenad Gucunski, and Trung H. Duong. "An algorithm for automatic localization and detection of rebars from GPR data of concrete bridge decks." Automation in Construction 89 (2018): 292-298.

[12] Xu, Xinjun, Yang Lei, and Feng Yang. "Railway subgrade defect automatic recognition method based on improved Faster R-CNN." Scientific Programming 2018 (2018).

[13] Tong, Zheng, Jie Gao, and Haitao Zhang. "Recognition, location, measurement, and 3D reconstruction of concealed cracks using convolutional neural networks." Construction and Building Materials 146 (2017): 775-787.

[14] R. Indrawijaya and P. A. BudimanRohman, "Cognitive Linear Trajectory on GPR Imaging Using Lightweight Machine Learning," 2023 International Conference on Radar, Antenna, Microwave, Electronics, and Telecommunications (ICRAMET), Bandung, Indonesia, 2023, pp. 436-439.

[15] Alvarez, Jean Kyle, and Sarath Kodagoda. "Application of deep learning image-to-image transformation networks to GPR radargrams for sub-surface imaging in infrastructure monitoring." 2018 13th IEEE Conference on Industrial Electronics and Applications (ICIEA). IEEE, 2018.

[16] Liu, Bin, et al. "GPRInvNet: Deep learning-based ground-penetrating radar data inversion for tunnel linings." IEEE Transactions on Geoscience and Remote Sensing 59.10 (2021): 8305-8325.

[17] Ji, Yintao, et al. "Deep neural network-based permittivity inversions for ground penetrating radar data." IEEE Sensors Journal 21.6 (2021): 8172-8183.

[18] Yang, Senlin, et al. "Defect segmentation: Mapping tunnel lining internal defects with ground penetrating radar data using a convolutional neural network." Construction and Building Materials 319 (2022): 125658.

[19] I. Goodfellow, Y. Bengio, and A. Courville. *Deep Learning* http://www.deeplearningbook.org, MIT Press, 2016. (accessed on 1 November 2020)

[20] C. Warren, A. Giannopoulos, and I. Giannakis. "Gprmax: open source software to simulate electromagnetic wave propagation for ground penetrating radar," *Computer Physics Communications*, vol. 209, pp. 163-170, 2016.

JET Template_2022_rev1.pdf

ORIGINALITY REPORT

24%	11%	23%	4%
SIMILARITY INDEX	INTERNET SOURCES	PUBLICATIONS	STUDENT PAPERS

PRIMARY SOURCES

1	Ratna Indrawijaya, P.A. BudimanRohman. "Cognitive Linear Trajectory on GPR Imaging Using Lightweight Machine Learning", 2023 International Conference on Radar, Antenna, Microwave, Electronics, and Telecommunications (ICRAMET), 2023 Publication	8%
2	Budiman P. A. Rohman, Masahiko Nishimoto, Kohichi Ogata. "Material Permittivity Estimation Using Analytic Peak Ratio of Air-Coupled GPR Signatures", IEEE Access, 2022 Publication	2%
3	Bo Li, Kele Xu, Dawei Feng, Haibo Mi, Huaimin Wang, Jian Zhu. "Denoising Convolutional Autoencoder Based B-mode Ultrasound Tongue Image Feature Extraction", ICASSP 2019 - 2019 IEEE International Conference on Acoustics, Speech and Signal Processing (ICASSP), 2019 Publication	2%

4	Budiman P. A. Rohman, Masahiko Nishimoto, Kohichi Ogata. "Reconstruction of Missing Ground-Penetrating Radar Traces Using Simplified U-Net", IEEE Geoscience and Remote Sensing Letters, 2021 Publication	2%
5	www.jurnalet.com Internet Source	1%
6	Budiman P.A. Rohman, Masahiko Nishimoto. "On the Instantaneous Phase of GPR Response for Concrete Relative Permittivity Estimation", 2019 8th Asia-Pacific Conference on Antennas and Propagation (APCAP), 2019 Publication	1%
7	www.researchgate.net Internet Source	1%
8	boristheses.unibe.ch Internet Source	1%
9	www.mdpi.com Internet Source	1%
10	Budiman P.A. Rohman, Masahiko Nishimoto. "Concrete Dielectric Constant Estimation Based on Analytic Signal Peak Ratio of GPR Response for Non-Destructive Inspection", IGARSS 2019 - 2019 IEEE International	1%

Geoscience and Remote Sensing Symposium, 2019
Publication

11	academic.oup.com Internet Source	1 %
12	Anastasia Aidini, Grigorios Tsagkatakis, Panagiotis Tsakalides. "Tensor Dictionary Learning with Representation Quantization for Remote Sensing Observation Compression", 2020 Data Compression Conference (DCC), 2020 Publication	<1 %
13	courses.grainger.illinois.edu Internet Source	<1 %
14	d-nb.info Internet Source	<1 %
15	core.ac.uk Internet Source	<1 %
16	hal-centralesupelec.archives-ouvertes.fr Internet Source	<1 %
17	informs-sim.org Internet Source	<1 %
18	"Machine Learning and Knowledge Discovery in Databases", Springer Science and Business Media LLC, 2017 Publication	<1 %

19	Budiman P.A. Rohman, Masahiko Nishimoto. "Estimation of Near-Surface Soil Moisture Through GPR Signal Processing Based on Multi-Scaled Spectral Feature Weighting", 2018 Progress in Electromagnetics Research Symposium (PIERS-Toyama), 2018 Publication	<1 %
20	Masahiko Nishimoto, Budiman P.A. Rohman, Kohichi Ogata. "Phase Parameter Extraction from UWB Radar Response for Non-destructive Inspection", 2021 International Symposium on Antennas and Propagation (ISAP), 2021 Publication	<1 %
21	Yuanzheng Wang, Hui Qin, Feng Miao. "A Multi-Path Encoder Network for GPR Data Inversion to Improve Defect Detection in Reinforced Concrete", Remote Sensing, 2022 Publication	<1 %
22	insightsociety.org Internet Source	<1 %
23	jees.kr Internet Source	<1 %
24	noesis.uis.edu.co Internet Source	<1 %
25	J. van der Kruk, T. Liu, A. Mozaffari, N. Gueting, A. Klotzsche, H. Vereecken, C.	<1 %

Warren, A. Giannopoulos. "GPR full-waveform inversion, recent developments, and future opportunities", 2018 17th International Conference on Ground Penetrating Radar (GPR), 2018
Publication

26	Ding Yang, Cheng Guo, Fanfan Wang, Longhao Xie, Ke Zhang, Yangchao Jin, Song Zhang, Qing Zhao. "PICGAN: Conditional adversarial neural network-based permittivity inversions for ground penetrating radar data", Journal of Applied Geophysics, 2023 Publication	<1 %

Exclude quotes	Off	Exclude matches	Off
Exclude bibliography	On		